Identifying the Stationary Viscous Flows Around a Circular Cylinder at High Reynolds Numbers

Christo I. Christov[1], Rossitza S. Marinova[2], and Tchavdar T. Marinov[1]

[1] Dept. of Math., University of Louisiana at Lafayette, LA 70504-1010, USA
[2] Dept. of Math. & Computing Sci., Concordia Univ. College of Alberta
7128 Ada Boul., Edmonton, AB, Canada T5B 4E4
christov@louisiana.edu, rossitza.marinova@concordia.ab.ca,
marinov@louisiana.edu

Abstract. We propose an approach to identifying the solutions of the steady incompressible Navier-Stokes equations for high Reynolds numbers. These cannot be obtained as initial-value problems for the unsteady system because of the loss of stability of the latter. Our approach consists in replacing the original steady-state problem for the Navier-Stokes equations by a boundary value problem for the Euler-Lagrange equations for minimization of the quadratic functional of the original equations. This technique is called Method of Variational Imbedding (MVI) and in this case it leads to a system of higher-order partial differential equations, which is solved by means of an operator-splitting method. As a featuring example we consider the classical flow around a circular cylinder which is known to lose stability as early as for Re = 40. We find a stationary solution with recirculation zone for Reynolds numbers as large as Re = 200. Thus, new information about the possible hybrid flow regimes is obtained.

1 Introduction

Navier-Stokes (N-S) equations, describing the flows of viscous incompressible liquid, exhibit reach phenomenology. Especially challenging are the flows for high Reynolds numbers when the underlying stationary flow loses stability and a complex system of transients takes place leading eventually to turbulence. In high Reynolds numbers regimes, the steady solution still exists alongside with the transients, but cannot be reached via numerical approximations of the standard initial-boundary value problem. It is important for the theory of the N-S model, to find the shape of the stationary solution even when it loses stability.

To illustrate the point of the present work, we consider the classical flow around a circular cylinder which has attracted the attention because of the early instability and intriguing transitions to turbulence. The flow becomes unstable as early as Re = 40 and the stationary regime is then replaced by an unsteady laminar flow called "Kármán vortex street, for $40 < \mathrm{Re} < 100$. With further increase of the Reynolds number the experiments show that the flow ends up in the turbulent regime around Re = 180. The appearance of 3D instabilities

I. Lirkov, S. Margenov, and J. Waśniewski (Eds.): LSSC 2007, LNCS 4818, pp. 175–183, 2008.

around Re = 200 was also confirmed by direct numerical simulations [9]. In spite of the many numerical calculations of the flow past a circular cylinder, accurate steady-state solutions for very large Reynolds numbers up to about 700 have been obtained only by Fornberg [7,8]. In his works, Fornberg reached high values of Reynolds number by means of a smoothing technique, which means that the problem is still not rigorously solved and is open to different approaches.

Although some agreement between theoretical, numerical and experimental results exists, there is a need for further work in this classical problem. To answer some of the above questions, we present here a new approach to identify the two-dimensional steady-state solution of N-S for the flow around a circular cylinder.

2 Problem Formulation

Consider the two-dimensional steady flow past a circular cylinder. The governing equations and the boundary conditions are presented in dimensionless form and polar coordinates (r, φ). The N-S equations read

$$\Omega = u_r \frac{\partial u_r}{\partial r} + \frac{u_\varphi}{r}\frac{\partial u_r}{\partial \varphi} - \frac{u_\varphi^2}{r} + \frac{\partial p}{\partial r} - \frac{1}{Re}\left(Du_r - \frac{2}{r^2}\frac{\partial u_\varphi}{\partial \varphi}\right) \tag{1}$$

$$\Phi = u_r \frac{\partial u_\varphi}{\partial r} + \frac{u_\varphi}{r}\frac{\partial u_\varphi}{\partial \varphi} + \frac{u_\varphi u_r}{r} + \frac{1}{r}\frac{\partial p}{\partial \varphi} - \frac{1}{Re}\left(Du_\varphi + \frac{2}{r^2}\frac{\partial u_r}{\partial \varphi}\right) \tag{2}$$

$$\Xi = \frac{\partial u_r}{\partial r} + \frac{u_r}{r} + \frac{1}{r}\frac{\partial u_\varphi}{\partial \varphi} = 0, \tag{3}$$

where $u_r = u(r, \varphi)$ and $u_\varphi = v(r, \varphi)$ are the velocity components parallel respectively to the polar axes r and φ; $p = p(r, \varphi)$ is the pressure. Furthermore, $D \equiv \frac{\partial^2}{\partial r^2} + \frac{1}{r}\frac{\partial}{\partial r} - \frac{1}{r^2} + \frac{1}{r^2}\frac{\partial^2}{\partial \varphi^2}$ is the so-called *Stokesian*. As usually, the Reynolds number ($\mathrm{Re} = U_\infty d/\nu$) is based on the cylinder diameter $d = 2a$, velocity at infinity U_∞, with ν standing for the kinematic coefficient of viscosity. In terms of dimensionless variables, the cylinder surface is represented by $r = 1$ and the velocity at infinity is taken equal to the unity, i.e., $U_\infty = 1$.

The boundary conditions reflect the non-slipping at the cylinder surface and the asymptotic matching with the uniform outer flow at infinity, i.e. at certain large enough value of the radial coordinate, say, r_∞. Due to the flow symmetry the computational domain may be reduced. Thus

$$\begin{aligned} u_r(1, \varphi) = u_\varphi(1, \varphi) = 0, \\ u_r(r_\infty, \varphi) = \cos\varphi, \quad u_\varphi(r_\infty, \varphi) = -\sin\varphi, \\ u_\varphi = \frac{\partial u_r}{\partial \varphi} = \frac{\partial p}{\partial \varphi} = 0 \quad \text{at} \quad \varphi = 0 \text{ and } \varphi = \pi. \end{aligned} \tag{4}$$

3 Method of Variational Imbedding (MVI)

For tackling inverse and incorrect problems Christov [1] developed the already mentioned MVI. Consider the imbedding functional of the governing equations (1)–(3)

$$\mathcal{J}(u_r, u_\varphi, p) = \int_0^\pi \int_1^\infty \left(\Phi^2 + \Omega^2 + X^2\right) r \, dr d\varphi. \tag{5}$$

The idea of MVI is to solve the equations of Euler-Lagrange, which are the necessary conditions of the minimization of the functional with respect to u_r, u_ϕ, and p, respectively

$$\left[\frac{1}{Re}\left(\frac{\partial^2}{\partial r^2} - \frac{\partial}{\partial r}\frac{1}{r} - \frac{1}{r^2} + \frac{1}{r^2}\frac{\partial^2}{\partial \varphi^2}\right) + \frac{\partial}{\partial r}u_r + \frac{\partial}{\partial \varphi}\frac{u_\varphi}{r} - \frac{\partial u_r}{\partial r}\right](r\Omega) - \left(\frac{1}{Re}\frac{2}{r^2}\frac{\partial}{\partial \varphi} + \frac{u_\varphi}{r} + \frac{\partial u_\varphi}{\partial r}\right)(r\Phi) + \left(\frac{\partial}{\partial r} - \frac{1}{r}\right)(r\Xi) = 0, \tag{6}$$

$$\left[\frac{1}{Re}\left(\frac{\partial^2}{\partial r^2} - \frac{\partial}{\partial r}\frac{1}{r} - \frac{1}{r^2} + \frac{1}{r^2}\frac{\partial^2}{\partial \varphi^2}\right) + \frac{\partial}{\partial r}u_r + \frac{\partial}{\partial \varphi}\frac{u_\varphi}{r} - \frac{1}{r}\frac{\partial u_\varphi}{\partial \varphi} - \frac{u_r}{r}\right](r\Phi) + \left(\frac{1}{Re}\frac{2}{r^2}\frac{\partial}{\partial \varphi} - \frac{1}{r}\frac{\partial u_r}{\partial \varphi} + \frac{2u_\varphi}{r}\right)(r\Omega) + \frac{1}{r}\frac{\partial}{\partial \varphi}(r\Xi) = 0. \tag{7}$$

$$\frac{\partial}{\partial r}(r\Omega) + \frac{1}{r}\frac{\partial}{\partial \varphi}(r\Phi) = 0. \tag{8}$$

The last equation after acknowledging the continuity equation becomes the well-known Poisson equation for pressure

$$\frac{1}{r}\frac{\partial}{\partial r}r\frac{\partial p}{\partial r} + \frac{1}{r^2}\frac{\partial^2 p}{\partial \varphi^2} - \frac{2}{r}\left(\frac{\partial u_\varphi}{\partial \varphi}\frac{\partial u_r}{\partial r} - \frac{\partial u_\varphi}{\partial r}\frac{\partial u_r}{\partial \varphi} + u_\varphi\frac{\partial u_\varphi}{\partial r} + u_r\frac{\partial u_r}{\partial r}\right) = 0. \tag{9}$$

To Eq. (4) we add also the so-called natural boundary conditions for minimization, which in this case reduce to $\Phi = \Omega = \Xi = 0$ for $r = a$ and $r = r_\infty$.

4 Interpretation of the MVI System and Implementation

Preserving the implicit nature of the system is of crucial importance because of the implicit nature of the boundary conditions, which involves the continuity equation but does not have explicit condition on pressure. To this end we introduce the vector unknown and right-hand sides

$$\boldsymbol{\theta} = \text{Column}[\Phi, u_\phi, \Omega, u_r, p], \quad \boldsymbol{F} = \text{Column}[F^\Phi, F^{u_\varphi}, F^\Omega, F^{u_r}, F^p], \tag{10}$$

where

$$F^{\Phi} = \frac{2}{Re \cdot r^2}\frac{\partial \Omega}{\partial \varphi} + u_r\frac{\partial \Phi}{\partial r} + \frac{u_\varphi}{r}\frac{\partial \Phi}{\partial \varphi} + \frac{2u_\varphi \Omega}{r} + \frac{1}{r}\frac{\partial X}{\partial \varphi} + \Phi\frac{\partial u_r}{\partial r} - \frac{\Omega}{r}\frac{\partial u_r}{\partial \varphi},$$

$$F^{u_\varphi} = \frac{2}{Re.r^2}\frac{\partial u_r}{\partial \varphi} - \left(u_r\frac{\partial u_\varphi}{\partial r} + \frac{u_\varphi}{r}\frac{\partial u_\varphi}{\partial \varphi} + \frac{u_\varphi u_r}{r}\right),$$

$$F^{\Omega} = -\frac{2}{Re.r^2}\frac{\partial \Phi}{\partial \varphi} + u_r\frac{\partial \Omega}{\partial r} + \frac{u_\varphi}{r}\frac{\partial \Omega}{\partial \varphi} - \frac{u_\varphi \Phi}{r} + \frac{\partial X}{\partial r} - \Phi\frac{\partial u_\varphi}{\partial r} - \Omega\frac{\partial u_r}{\partial r},$$

$$F^{u_r} = -\frac{2}{Re.r^2}\frac{\partial u_\varphi}{\partial \varphi} - \left(u_r\frac{\partial u_r}{\partial r} + \frac{u_\varphi}{r}\frac{\partial u_r}{\partial \varphi} - \frac{u_\varphi^2}{r}\right),$$

$$F^{p} = -\frac{2}{r}\left(\frac{\partial u_\varphi}{\partial \varphi}\frac{\partial u_r}{\partial r} - \frac{\partial u_\varphi}{\partial r}\frac{\partial u_r}{\partial \varphi} + u_\varphi\frac{\partial u_\varphi}{\partial r} + u_r\frac{\partial u_r}{\partial r}\right).$$

We denote the linear differential operators as $\Lambda_r = \frac{\partial}{\partial r}$, $\Lambda_\varphi = \frac{1}{r}\frac{\partial}{\partial \varphi}$ and

$$\Lambda_{rr} = \frac{1}{r}\frac{\partial}{\partial r}r\frac{\partial}{\partial r}, \quad \hat{\Lambda}_{rr}\frac{1}{\mathrm{Re}}(\lambda_{rr} - \frac{1}{r^2}), \quad \Lambda_{\varphi\varphi} = \frac{1}{r^2}\frac{\partial^2}{\partial \varphi^2}, \quad \hat{\Lambda}_{\phi\phi}\frac{1}{\mathrm{Re}}\Lambda_{\phi\phi}.$$

Then the matrix operators have the form

$$\mathbb{L}_1 = \begin{pmatrix} \hat{\Lambda}_{rr} & 0 & 0 & 0 & 0 \\ \frac{1}{2} & \hat{\Lambda}_{rr} & 0 & 0 & 0 \\ 0 & 0 & \hat{\Lambda}_{rr} & 0 & 0 \\ 0 & 0 & \frac{1}{2} & \hat{\Lambda}_{rr} & -\Lambda_r \\ 0 & 0 & 0 & 0 & \Lambda_{rr} \end{pmatrix} \quad \mathbb{L}_2 = \begin{pmatrix} \hat{\Lambda}_{\varphi\varphi} & 0 & 0 & 0 & 0 \\ \frac{1}{2} & \hat{\Lambda}_{\varphi\varphi} & 0 & 0 & -\Lambda_\varphi \\ 0 & 0 & \hat{\Lambda}_{\varphi\varphi} & 0 & 0 \\ 0 & 0 & \frac{1}{2} & \hat{\Lambda}_{\varphi\varphi} & 0 \\ 0 & 0 & 0 & 0 & \Lambda_{\varphi\varphi} \end{pmatrix}. \tag{11}$$

The original system under consideration is non-linear but the way we introduced the non-homogeneous vector $\boldsymbol{F}$ hints at the obvious linearization: we invert just the linear operators $\mathbb{L}_i$. The iterative procedure is based on the operator splitting and the novel element here is that we perform the splitting in the vector form of the system. We generalize the second Douglas scheme [6], sometimes called the scheme of stabilizing correction (see also [15]) in the form

$$\frac{\boldsymbol{\theta}^{n+\frac{1}{2}} - \boldsymbol{\theta}^n}{\sigma} = \mathbb{L}_1\boldsymbol{\theta}^{n+\frac{1}{2}} + \mathbb{L}_2\boldsymbol{\theta}^n + \boldsymbol{F}^n, \; \frac{\boldsymbol{\theta}^{n+1} - \boldsymbol{\theta}^{n+\frac{1}{2}}}{\sigma} = \mathbb{L}_2\boldsymbol{\theta}^{n+1} - \mathbb{L}_2\boldsymbol{\theta}^n, \tag{12}$$

or, which is the same

$$(I - \sigma\mathbb{L}_1)\boldsymbol{\theta}^{n+\frac{1}{2}} = (I + \sigma\mathbb{L}_2)\boldsymbol{\theta}^n + \sigma\boldsymbol{F}^n, \quad (I - \sigma\mathbb{L}_2)\boldsymbol{\theta}^{n+1} = \boldsymbol{\theta}^{n+\frac{1}{2}} - \tau\mathbb{L}_1\boldsymbol{\theta}^n, \tag{13}$$

where σ is the increment of the artificial time, and L_1 and L_2 are one-dimensional operators. The superscript n stands for the "old" time stage, $n + \frac{1}{2}$ for the intermediate step and $(n + 1)$ – for the "new" step.

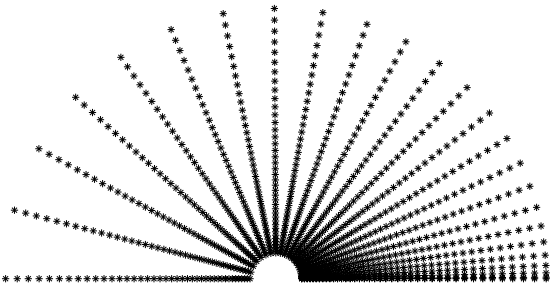

Fig. 1. Grid-points distribution

The scheme of stabilizing correction approximates in the full time step the backward Euler scheme and, therefore, for linear systems it is unconditionally stable. For the nonlinear problem under consideration it retains its strong stability allowing us to choose rather large time increments σ and to obtain the steady solution with fewer steps with respect to the artificial time.

We chose finite difference method with symmetric differences for the spatial discretization. The number of points in r direction is M, and in ϕ direction – N. The pointwise values of the set functions that comprise the vector of unknowns $\boldsymbol{\theta}$ are arranged in the same order and as a result we get a vector of dimension $5M$ or $5N$. Note that each of the five equations of the system on each half-time step is represented by a tri-diagonal algebraic system. However, in order to preserve the coupling, we render it to an eleven-diagonal system for the properly arranged vector of unknowns. Thus we are able to impose the boundary conditions as they stand: two conditions on a velocity component and no conditions on pressure. As a result, the scheme is fully implicit with respect to the boundary conditions which is extremely beneficial for the stability. We have used this idea in different algorithms for solving the N-S equation and it proved crucial for the effectiveness of the scheme ([11,13]).

We use both uniform and non-uniform grids in order to evaluate better the approximation properties of the algorithm. The special non-uniform grid

$$r_i = \exp\left[(i-1)\frac{R-1}{N_r-1}\right], \quad \varphi_j = \frac{1}{\pi}\left[(j-1)\frac{\pi}{N_\varphi - 1}\right]^2,$$

takes into account the *a-priori* information of the regions of large gradients of the flow and it is presented in Fig. 1. The grid is staggered for p in direction φ, which ensures the second order of approximation of the pressure boundary condition on the lines of symmetry $\varphi = 0$ and $\varphi = \pi$. For the same reason the grid for u_r and Ω is staggered in both directions. The grid-lines in direction r are denser near the cylinder and sparser far from the body. The grid in direction φ is chosen to be denser behind the body. All boundary conditions are imposed implicitly with the second order of approximation.

Table 1. Results for C_p, C_f, C_D and $p(1,\pi) - p(1,0)$, obtained on uniform grid with different h_φ and h_r and fixed $\mathrm{Re} = 4$, $r_\infty = 16$

Grid	C_p	C_f	C_D	$p(1,\pi) - p(1,0)$
51×26	2.9732	2.3695	5.3427	1.9533
101×51	2.9652	2.5203	5.4855	1.9420
201×101	2.9623	2.5812	5.5435	1.9384

5 Scheme Validation

Since we use artificial time and splitting scheme, the first thing to verify is that the result for the steady problem does not depend on the time increment. We computed the solution for $\mathrm{Re} = 40$ on the non-uniform grid using three different artificial-time steps: $\sigma = 0.1,\ 0.01,\ 0.001$ and have found that after the stationary regime is reached, the results for the three different time steps do not differ more than 10^{-6}, which is of the order of the criterion of convergence of the iterations.

The next important test is the verification of the spatial approximation of the scheme. We have conducted a number of calculations with different values of mesh parameters in order to confirm the practical convergence and the approximation of the difference scheme. In these tests, the mesh is uniform in both directions with spacings h_r and h_φ. The uniform grid is adequate only for $\mathrm{Re} \leq 40$, but it is enough for the sake of this particular test. Results for some of the important characteristics as obtained with different spacings h_r and h_φ are presented in Table 1 for $r_\infty = 16$ and $\mathrm{Re} = 4$.

The third test is to find the magnitude of r_∞ for which the solution is adequate. Clearly, the boundary conditions should be posed as close to the body as possible to save computational resources. On the other hand, the boundary condition has to be at a sufficiently large distance from the end of the separation bubble. We examined the dependence of solution on r_∞ for $\mathrm{Re} = 20$ when a separation is known to exist. Table 2 presents some of the flow characteristics as computed with different r_∞. The impact of r_∞ is significant for small values, but the results converge with the increase of r_∞. It is clear that $r_\infty \geq 20$ presents a large enough computational domain, so the further change of the parameters with the increase of r_∞ is insignificant.

Table 2. Separation angle φ_{sep}, bubble length L and width W, pressure drag coefficient C_p, friction drag coefficient C_f, difference $p_{\mathrm{diff}} = p(1,\pi) - p(1,0)$, $\max|\omega(1,\varphi_j)|$ as functions of r_∞ grid for $Re = 20$ and uniform grid with $h_r = 0.07$ and $h_\varphi = \pi/100$

r_∞	φ_{sep}	L	W	C_p	C_f	p_{diff}	$\max\|\omega(1,\varphi_j)\|$
4.5	0.636(36.45°)	1.81	0.581	2.5105	1.4345	1.8219	6.61
8	0.717(41.06°)	2.35	0.689	1.7368	1.0701	1.3945	5.15
15	0.744(42.63°)	2.68	0.728	1.4208	0.9098	1.0706	4.45
22	0.749(42.94°)	2.78	0.749	1.3308	0.8621	1.0056	4.24

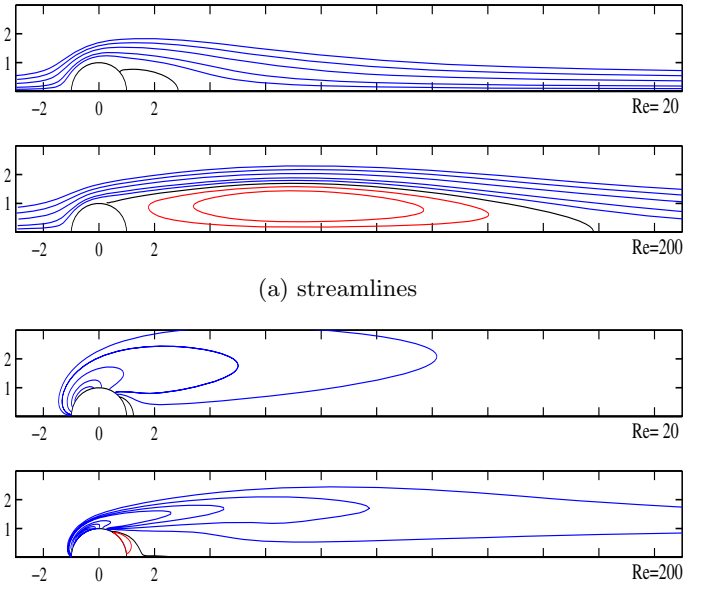

(a) streamlines

(b) vorticity isolines

Fig. 2. Flow patterns for $Re = 20$ and $Re = 200$

6 Results

The above described algorithm yielded stable computations for Reynolds numbers as high as Re = 200, much higher than the threshold of instability, which is believed to be around Re = 40. In Fig. 2 we present the streamlines and the vorticity distribution for two Reynolds numbers.

Our results indicate that the flow separation and formation of a recirculation zone behind the body appears first for Re = 10. The length of the wake (separation bubble) becomes longer and wider with increasing the Reynolds number. Our numerical results with Re = 20 on a non-uniform grid ($r_\infty \approx 88$) differ less than 10% from those with the uniform grid 301×101, where $r_\infty = 22$. The reason for the relatively high discrepancies are the large spacings of the uniform grid near the surface of the body, in particular in the r-direction, where $h_r = 0.07$. In this case the value of $r_\infty = 22$ is not sufficiently large as well.

Fornberg [7] has found that the wake bubble (region of recirculating flow) has eddy length $L \propto \mathrm{Re}$, width $W \propto \sqrt{\mathrm{Re}}$ up to Re = 300, and $W \propto \mathrm{Re}$ beyond that. Smith [14] and Peregrine [12] have performed theoretical work which gives a fresh interpretation of Fornberg's results. There are several discrepancies between the theories of Smith and Peregrine, some of which are a matter of interpretation. These are unlikely to be resolved without further analysis and computational work. Our works is a contribution to this direction. The characteristics of the wake are presented in Fig. 3. Similarly, the values of the separation

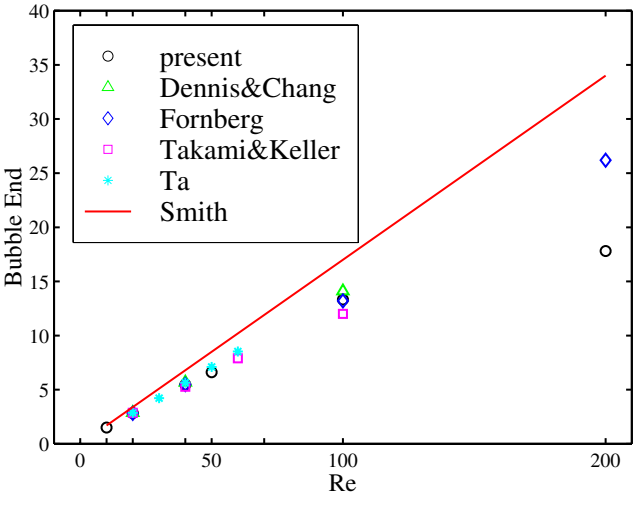

Fig. 3. Characteristics of the wake

angle φ_{sep} measured from the rear stagnation point are in good agreement with the computations of [5].

7 Conclusion

The results of the present work validate the proposed approach in the sense that the possibility of finding the steady solution even when it is unstable physically is clearly demonstrated. It should be noted that within the truncation error, our approach is exact, and no additional procedures, like filtering or smoothing, are applied. Steady solutions have been computed in primitive variables formulation for $\text{Re} \leq 200$. The Reynolds numbers range of our work is wider than the others with the exception of Fornberg's work in stream function/vorticity function formulation, where an *ad hoc* smoothing is used.

Acknowledgement

The work of R. Marinova was partially supported by a grant from MITACS.

References

1. Christov, C.I.: A method for identification of homoclinic trajectories. In: Proc. 14th Spring Conf. Union of Bulg, Mathematicians, Sunny Beach, pp. 571–577 (1985)
2. Christov, C.I., Marinova, R.S.: Numerical investigation of high-Re stationary viscous flow around circular cylinder as inverse problem. Bulg. J. Meteorology Hydrology 5(3–4), 105–118 (1994)

3. Christov, C.I., Marinova, R.S.: Implicit scheme for Navier-Stokes equations in primitive variables via vectorial operator splitting. In: Griebel, M., et al. (eds.) Notes on Num. Fluid Mech., Vieweg, Germany, vol. 62, pp. 251–259 (1997)
4. Christov, C.I., Marinova, R.S.: Numerical solutions for steady flow past a circular cylinder via method of variational imbedding. Annuaire de l'Universite de Sofia 'St. Kl. Ohridski' 90, 177–189 (1998)
5. Dennis, S.C.R., Gau–Zu, C.: Numerical solutions for steady flow past a circular cylinder at Reynolds numbers up to 100. J. Fluid Mech. 42(3), 471–489 (1970)
6. Douglas, J., Rachford, H.H.: On the numerical solution of heat conduction problems in two and three space variables. Trans, Amer. Math. Soc. 82, 421–439 (1956)
7. Fornberg, B.: Steady flow past a circular cylinder up to Reynolds number 600. J. Comput. Phys. 61, 297–320 (1985)
8. Fornberg, B.: Steady incompressible flow past a row of circular cylinders. J. Fluid Mech. 225, 655–671 (1991)
9. Karniadakis, G.E., Triantafyllou, G.S.: Three-dimensional dynamics and transition to turbulence in the wake of bluff objects. J. of Fluid Mech. 238, 1–30 (1992)
10. Mallison, G.D., de Vahl Davis, G.: The method of false transients for the solution of coupled elliptic equations. J. Comp. Phys. 12, 435–461 (1973)
11. Marinova, R.S., Christov, C.I., Marinov, T.T.: A fully coupled solver for incompressible Navier-Stokes equations using coordinate operator splitting. Int. J. Comp. Fluid Dynamics 17(5), 371–385 (2003)
12. Peregrine, D.H.: A note on steady high-Reynolds-number flow about a circular cylinder. J. Fluid Mech. 157, 493–500 (1985)
13. Smagulov, S., Christov, C.I.: An iterationless implementation of boundary condition for vorticity function (preprint). Inst. Theor. Appl. Mech., Russian Acad. Sci., Novosibirsk 20 (1980) (in Russian)
14. Smith, F.T.: A structure for laminar flow past a bluff body at high Reynolds number. J. Fluid Mech. 155, 175–191 (1985)
15. Yanenko, N.N.: Method of Fractional Steps. Gordon and Breach, London (1971)